JOURNAL OF THERMOPHYSICS AND HEAT TRANSFER
Vol. 16, No. 1, January–March 2002

Numerical Simulation of High-Temperature Gas Flows in a Millimeter-Scale Thruster

A. A. Alexeenko* and D. A. Levin†
Pennsylvania State University, University Park, Pennsylvania 16802
S. F. Gimelshein‡
George Washington University, Washington, D.C. 20052
R. J. Collins§
University of Minnesota, Minneapolis, Minnesota 55455
and
G. N. Markelov¶
Institute of Theoretical and Applied Mechanics, 630090, Novosibirsk, Russia

High-temperature nozzle flows at low Reynolds numbers are studied numerically by the direct simulation Monte Carlo method. Modeling results are compared with the experimental data on the specific impulse efficiency of a heated nitrogen flow at $Re = 1.78 \times 10^2$–4.09×10^2. Good agreement between modeling and data was observed for nonadiabatic wall conditions. The relative influence of three major thrust loss factors—flow divergence, surface friction, and heat transfer in axisymmetric and three-dimensional nozzles—is estimated for stagnation temperatures of 300, 1000, and 2000 K and $Re = 2.05 \times 10^2$. For a stagnation temperature of 1000 K, the specific impulse is 50% larger than in the cold gas case (300 K), whereas the efficiency is 10% lower as a result of heat-transfer losses of the same magnitude as friction losses. Axisymmetric conical nozzle thrust performance was studied for a hydrogen-air propellant over a range of $Re = 2 \times 10^2$–2×10^3. It is found that vibrational relaxation could be a significant factor in the simulation of such flows.

Nomenclature

A = exit to throat area ratio
F = thrust, N
I_{sp} = specific impulse, s
Kn = Knudsen number
p = pressure, Pa
R = radius
Re = Reynolds number
T = temperature, K
u = velocity, m/s
Z = relaxation number
α = accommodation coefficient, expansion angle
η = specific impulse efficiency, I_{sp}/I^*_{sp}
ρ = mass density, kg/m^3

Subscripts

i = incident
r = reflected, rotational
t = throat
v = vibrational
w = wall
x = component along the nozzle axis
τ = tangential
0 = stagnation

Superscript

$*$ = ideal vacuum conditions

Received 2 April 2001; revision received 31 July 2001; accepted for publication 2 August 2001.

*Graduate Assistant, Aerospace Engineering Department, 233 Hammond Building; alexeenko@psu.edu. Student Member AIAA.
†Associate Professor, Aerospace Engineering Department, 233 Hammond Building; dalevin@psu.edu. Senior Member AIAA.
‡Senior Research Scientist, Chemistry Department, 725 21st Street N.W.; gimel@gwu.edu. Member AIAA.
§Professor Emeritus, Department of Electrical and Computer Engineering; currently Retired, 8306 Melody Court, Bethesda, MD 20817; swbemac@aol.com. Senior Member AIAA.
¶Senior Research Scientist, 4/1 Institutskaya Street; markelov@itam.nsc.ru.

I. Introduction

THE utility of low-thrust micronozzles to the new generation of space vehicles has been discussed by many workers.[1,2] Different micropropulsion concepts are being considered for space applications such as cold gas thrusters, resistojets, and others. The cold gas thrusters operating at low Reynolds numbers, $Re < 1.5 \times 10^3$, have low specific impulse (a typical value is 65–75 s for nitrogen propellant) as a result of significant viscous losses. Higher specific impulse values can be achieved when a heated gas flow is generated (resistojets are an example). Recently, a fabrication of a microturbine driven by a bipropellant microcombustor using microelectromechanical systems (MEMS) technology has been reported.[3] In that work temperatures on the order of 1000 K were obtained in a silicon-based hydrogen-air combustor of dimensions of several millimeters. This last result raised the possibility of fabricating new microrocket engines. The modeling of high-temperature gases in the nozzle region will be discussed in this work.

System designers need a general capability to model micronozzle performance for different shapes and propellants as will be dictated by the specific mission requirements. In this connection the accurate modeling of low-thrust nozzles becomes indispensable. The thrust from a micronozzle operating in a low-Reynolds-number regime cannot be calculated using conventional computational fluid dynamics techniques because the continuum assumption is not applicable throughout the flow. The Knudsen number based on the nozzle throat diameter is of the order of 10^{-3} and grows several orders of magnitude at the nozzle exit. At such a high degree of rarefaction, a kinetic, that is, microscopic, approach has to be applied. The most powerful and widely used numerical kinetic approach is the direct simulation

Monte Carlo (DSMC) method. The DSMC and continuum methods were used for performance evaluation of a cold gas flow in axisymmetric micronozzles in, for example, Refs. 4–6. The DSMC modeling of a cold gas flow in micronozzles of three-dimensional geometric configurations was considered in Refs. 7 and 8. The DSMC method has been employed by Zelesnik et al. for the numerical study of cold and heated gas flows in axisymmetric nozzles of different geometric shapes in Ref. 9. They reported that for higher than 300 K gas temperatures the nozzle efficiency is less than 50% as a result of heat losses in the viscous flow at $Re = 90$. The main objective of the present work is the modeling of high-temperature axisymmetric and three-dimensional nozzle flows at higher Reynolds numbers, $Re = 2 \times 10^2$–2×10^3, with an emphasis on the examination of gas-surface interaction effects on the nozzle performance. As was discussed in earlier work,[8] the higher Reynolds number and the three-dimensionality of the flow increase the difficulty of obtaining an accurate DSMC solution independent of particle correlations. The numerical techniques presented in Ref. 8 are further expanded in the research discussed here.

Using DSMC techniques, the specific impulse efficiency (the ratio of specific impulse to ideal vacuum specific impulse) for a nitrogen flow at a stagnation temperature of 1033 K and low Reynolds numbers is calculated and compared with experimental data.[10] This comparison with the data provides credibility for the application of numerical modeling for anticipating new configurations yet to be fabricated or tested. For an accurate estimation of micronozzle thrust performance by the DSMC method, a number of important simulation issues are considered in the paper. Among these are the modeling of heat transfer to the nozzle wall and thermal relaxation of gas molecules, critical in a high-temperature viscous nozzle flow. To understand the variation of the nozzle flow caused by throat and wall-temperatures and surface models, both cold- and high-temperature gas flows will be investigated. The impact of vibrational-translational energy transfer in the nozzle flows containing polyatomic gases is also investigated, and results for the thruster performance are discussed.

II. Gas-Surface Interactions Models and Numerical Method

The DSMC method[11] has been applied in this work to obtain numerical solutions for low-Reynolds-number nozzle flows. A DSMC-based software SMILE[12] is used for all computations. This code uses the majorant frequency scheme[13] of the DSMC method for modeling of collisional process. The intermolecular potential is assumed to be the variable soft-sphere (VSS) model.[14] The Larsen–Borgnakke model[15] with discrete rotational and vibrational energies is used to model the energy exchange between the translational and internal modes. Temperature-dependent rotational and vibrational collision numbers Z_r and Z_v are assumed, and

$$Z_r = \tau_r/\tau_c, \qquad Z_v = \tau_v/\tau_c$$

Here, the VSS expression [11] is used for the collisional relaxation time τ_c, Eq. (45) from the work of Parker[16] is used for the rotational relaxation time τ_r, and the Millikan–White expression [Eq. (3) in Ref. 17] is taken for the vibrational relaxation time τ_v. The DSMC correction factors[18,19] for Z_r and Z_v were employed.

The Maxwell model of gas-surface interactions is used to model the momentum and heat transfer to the wall. The model assumes that a fraction $(1 - \alpha_d)$ of incident particles is reflected specularly while the remaining fraction α_d experiences a diffuse reflection on the wall. The parameter α_d is the tangential momentum accommodation coefficient

$$\alpha_d = \frac{P_{i\tau} - P_{r\tau}}{P_{i\tau}}$$

where P_τ is the tangential momentum. The diffuse reflection implies that the particle translational and internal energies are distributed according to the Maxwell–Boltzmann distribution subject to the energy accommodation coefficient α_E

Table 1 Summary of cases considered

Flow conditions	Designation
Comparison with experiment—axisymmetric conical nozzle, $A = 100$, $\alpha = 20$ deg, N_2	
$T_0 = 1000$ K	Different Reynolds numbers
Effect of temperature—axisymmetric conical nozzle, $A = 100$, $\alpha = 15$ deg, N_2	
$T_0 = 300$ K	Cold gas, set 1
$T_0 = 1000$ K	Heated gas, set 2
$T_0 = 2000$ K	High-temperature, set 3
Effect of temperature—three-dimensional high-aspect ratio	
$T_0 = 300$, 1000 K	
Gas-Surface models	
$\alpha_d = 0$, $\alpha_E = 0$	Case 1, specular reflection, adiabatic wall
$\alpha_d = 1$, $\alpha_E = 0$	Case 2, diffuse reflection, adiabatic wall
$\alpha_d = 1$, $\alpha_E = 1$	Case 3, diffuse reflection, full energy accommodation at a constant T_w
Hydrogen-air propellant—axisymmetric conical nozzle, $A = 100$, $\alpha = 15$ deg	
$P_0 = 0.1$, 0.05, 1.0 atm	
Thermal relaxation	
$Z_V(T)$, $Z_R(T)$	Temperature dependent
$Z_V = 100$, $Z_R = 5$	Moderate relaxation
$Z_V = Z_R = 1$	Fast relaxation

$$\alpha_E = (E_i - E_r)/(E_i - E_w)$$

where E_w is the energy that the reflected molecule would acquire if there were a thermal equilibrium between the wall and the gas. Thus, the case $\alpha_E = 0$ corresponds to adiabatic conditions and a wall temperature need not be specified. For $\alpha_E > 0$ a constant wall temperature is used. The model cases and flow conditions considered in the paper are summarized in Table 1.

Adaptive two-level grids for collisions and macroparameter sampling have been used in the DSMC calculations. Total number of collision cells varied from 3×10^4 for $Re = 2 \times 10^2$ to 6×10^5 for $Re = 2 \times 10^3$ in axisymmetric case. The total sampling size in all cases was bigger than 5×10^5 for each collisional cell.

III. Comparison with Experimental Data

A comparison with available experimental data[10] has been performed to validate the DSMC models and algorithms. Results of the comparison are presented in this section. Measurements of specific impulse efficiency of an axisymmetric nozzle for a range of low Reynolds numbers have been reported in Ref. 10. In that work centimeter scale nozzles have been tested over a range of chamber pressure values in such a way that high enough thrust levels are produced to be measured with precision. The gas temperature in the static chamber was elevated by a resistance heating element, and nitrogen gas expansion through nozzles of different geometries was studied. Results of the measurements were also compared in Ref. 10 with the compressible boundary-layer (BL) approximation calculated according to the Cohen–Reshotko procedure.[20] A zero heat transfer to the wall was assumed in the approximation of Ref. 10.

To compare with the experimental data, nitrogen flow at a stagnation temperature of $T_0 = 1033$ K through an axisymmetric conical nozzle with an expansion angle of 20 deg, and an area ratio of 100 is modeled for different Reynolds numbers, $Re = 1.78 \times 10^2$, 3.06×10^2, 4.09×10^2. The full accommodation of tangential momentum ($\alpha_d = 1$) and different energy surface models has been used in the DSMC calculations. The calculated translational temperature contours for $Re = 1.78 \times 10^2$ are plotted in Fig. 1 for three cases: adiabatic conditions ($\alpha_E = 0$) and two different wall temperatures $T_w = 300$ and 500 K ($\alpha_E = 1$). The calculated temperature field solution is sensitive to the type of wall conditions in the latter two cases, and the difference in translational temperature between adiabatic conditions and constant T_w at the nozzle exit is about 25%.

Table 2 Calculated performance characteristics for nitrogen flow in axisymmetric conical nozzle, $A = 100$, $\alpha = 20$ deg, $T_0 = 1033$ K, $T_w = 500$ K, $\alpha_E = 1$, $\alpha_d = 1$

Re	F, mN	I_{sp}, s	η, %
178	5.48	116.2	80.7
306	8.70	119.9	83.3
409	11.76	122.4	85.0

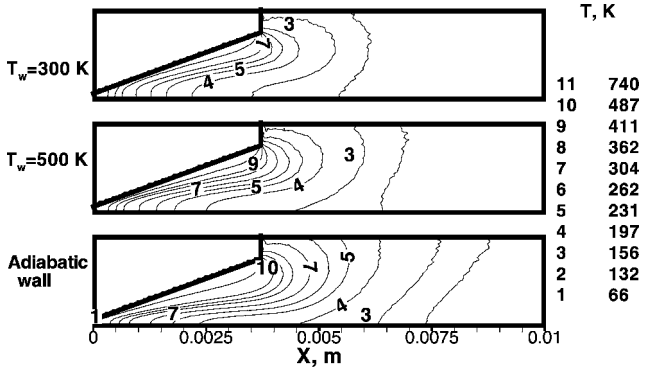

Fig. 1 Translational temperature contours for $Re = 1.78 \times 10^2$ with different wall conditions for $T_0 = 1033$ K, $A = 100$, $\alpha = 20$ deg, top and middle—$\alpha_E = 1$, bottom—$\alpha_E = 0$.

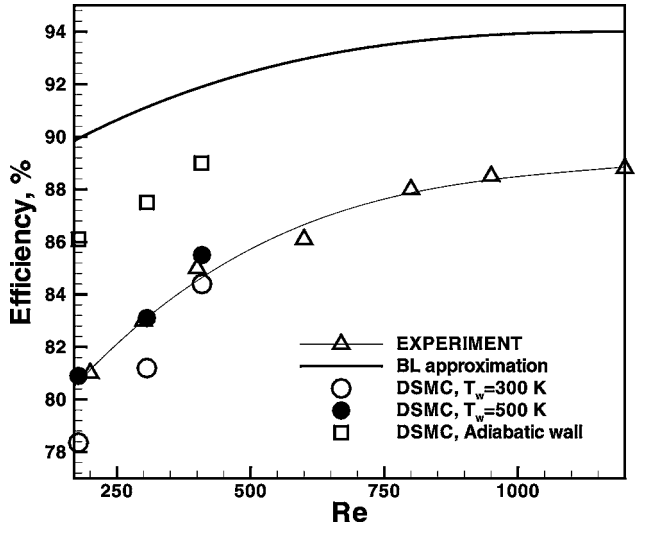

Fig. 2 Calculated and measured efficiency for axisymmetric conical nozzle.

The measured and calculated axisymmetric nozzle efficiencies are plotted in Fig. 2. Although the calculated thrust increases by a factor of two with an increase in the Reynolds number from 2×10^2 to 4×10^2, the calculated efficiency growth is strongly hampered by viscous losses. The total efficiency rise in the experiment is only 5%, and there is a good agreement with the computational results shown in Table 2. The BL approximation used in Ref. 10 predicts a decrease in nozzle efficiency when the Reynolds number decreases. But the efficiency is overestimated because the heat transfer to the wall has been neglected in this approximation. Note, the wall temperature was not given in Ref. 10 but is expected to be higher than room temperature 300 K and significantly lower than the stagnation temperature of 1033 K. That is why the DSMC computations were performed for constant wall temperatures of 300 and 500 K and an adiabatic wall ($\alpha_d = 1$, $\alpha_E = 0$). The DSMC results are in good agreement with the experimental data for the case of $T_w = 500$ K, for which the calculated points fall within 0.5% from the experimental ones. They are somewhat lower (within 2.5%) for a wall temperature of 300 K and significantly overestimate the data for the assumption of an adiabatic wall. The prediction of nozzle performance is therefore sensitive to the choice of wall temperature and energy accommodation coefficient in the surface model. The influence of the energy and momentum accommodation coefficients on the nozzle flow for different temperature regimes is further analyzed in the next section.

IV. Effects of the Accommodation Coefficient and Temperature Regime

A study of influence of the surface energy and momentum accommodation coefficients on the simulation results for both cold and heated nozzle flows was carried out. Molecular nitrogen expanding through a conical micronozzle at a low Reynolds number was used for this purpose. The expansion half-angle is 15 deg, the throat radius is 150 μm, and the area ratio is 100. Three sets of chamber conditions were chosen to study low- and high-temperature flows at the same Reynolds number (they will be referred to as cold, heated, and high-temperature flows). Throat conditions for these sets are calculated from chamber conditions for an isentropic expansion and are listed in Table 3. In all three cases the Knudsen number based on the nozzle diameter is 2.77×10^{-3}, and the Reynolds number is 4.105×10^2.

For these flow conditions different values of accommodation coefficients in the Maxwell gas-surface interaction model were used (see Table 1). Case 1 corresponds to an ideally smooth surface with no momentum and energy transfer between the gas flow and the wall. The second case is the diffuse reflection with an adiabatic wall, i.e., an average tangential momentum of reflected particles is equal to zero and no energy transfer occurs during particle-surface collisions. The last case implies both momentum and energy transfer with the wall at a constant temperature of 300 K.

Cold Gas Flow

Consider first a cold gas flow through the nozzle with set 1 conditions (see Table 3). The resulting translational temperature contours are plotted in Fig. 3 for the three types of gas-surface interactions. In case 1, where the tangential momentum of molecules that collided with the wall is unchanged, there is no surface friction, and no heat transfer occurs to the wall. No BL develops at the wall in this case. In cases 2 and 3 the translational temperature in the boundary layer near the wall is higher than that in the core flow because of viscous dissipation of the flow kinetic energy. The translational temperature profiles along the nozzle centerline are plotted in Fig. 4. The difference between the results for an adiabatic wall (case 2) and a constant wall temperature (case 3) is small because the wall temperature is equal to the stagnation temperature of the flow. There is a local maximum of temperature observed at the nozzle exit for the last two cases, which is connected with the significant growth of the boundary layer.

Table 4 gives calculated nozzle performance characteristics for set 1. The specific impulse in case 1 is very close to the ideal nozzle theory prediction. In cases 2 and 3 the efficiency of the nozzle is

Table 3 Flow conditions

Set	1	2	3
T_0, K	300	1,000	2,000
T_t, K	250	833	1,667
p_t, Pa	5,270	23,820	56,351
u_t, m/s	322.4	586.2	819.2

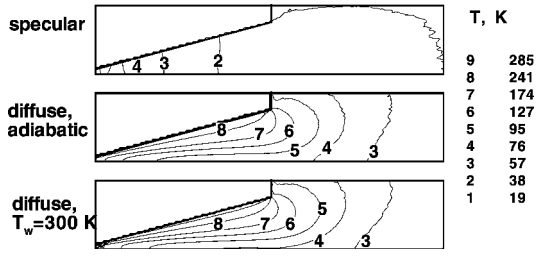

Fig. 3 Translational temperature fields for set 1.

Table 4 Calculated performance characteristics for axisymmetric conical nozzle, $A = 100$, $\alpha = 15$ deg, N_2

	$T_0 = 300$ K		$T_0 = 1000$ K		$T_0 = 2000$ K	
Case	I_{sp}, s	η, %	I_{sp}, s	η, %	I_{sp}, s	η, %
Ideal	76.5	100	142.1	100	201.0	100
1	74.8	97.8	138.2	97.3	194.5	96.7
2	64.2	79.8	117.6	82.7	166.8	83.0
3	65.5	83.1	103.8	73.0	141.3	70.3

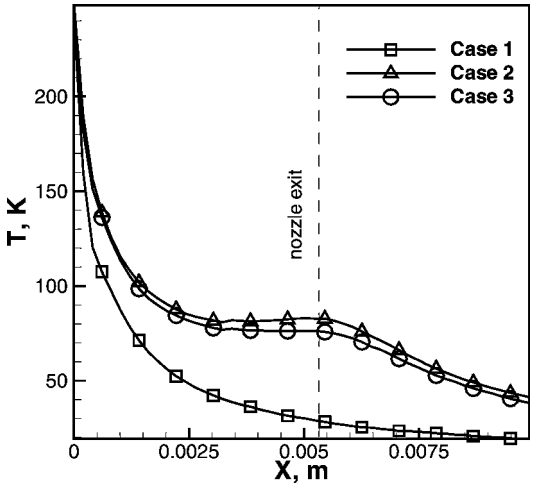

Fig. 4 Translational temperature along the nozzle centerline for set 1.

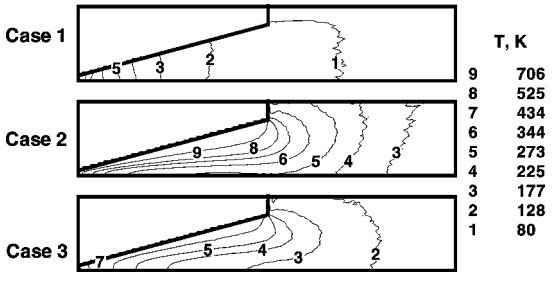

Fig. 5 Translational temperature fields for set 2. Case 1, specular reflection; case 2, diffuse reflection, adiabatic wall; case 3, diffuse reflection, $T_w = 300$ K.

about 20% lower. The difference in I_{sp} between the results for the adiabatic wall and a constant wall temperature is small because, again, the wall temperature is equal to the stagnation temperature of the flow.

Heated Flow

The structure of a heated flow for different accommodation coefficients models is shown in Fig. 5. Comparison with Fig. 3 shows that for a heated flow the flowfield structure is more sensitive to the gas-surface model than for a cold gas. The temperature near the wall is maximum for case 2. This is caused by the viscous dissipation of kinetic energy on the wall where the flow velocity drops and temperature increases. In this case there is no heat transfer to the wall, and the temperature is higher than in case 3, where it decreases as a result of heat losses. The influence of the heat losses in case 3 is more evident in the translational temperature profiles along the nozzle axis, shown in Fig. 6. In contrast to the cold gas flow (Fig. 4), the calculated translational temperature for the heated flow is sensitive to the choice of the energy accommodation coefficient α_E.

The calculated thrust performance of the 1000 K heated nozzle flow is given in the Table 4 for different accommodation parameters. In contrast to the cold gas flow case, there is a clear trend in efficiency as a function of gas-surface losses. The thrust is a maximum in case 1 because no heat and momentum losses occur at the wall. In case 2

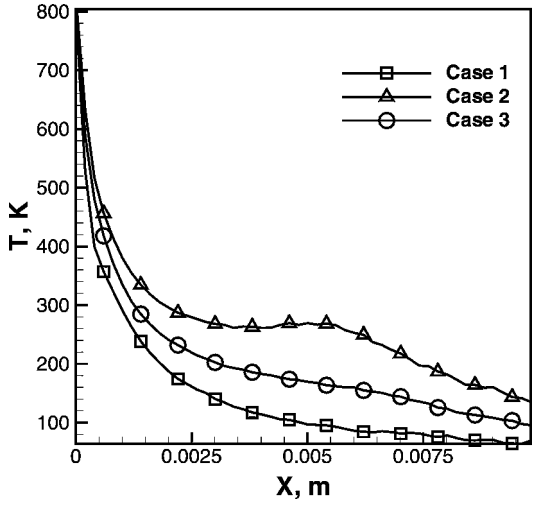

Fig. 6 Translational temperature along the nozzle centerline for set 2.

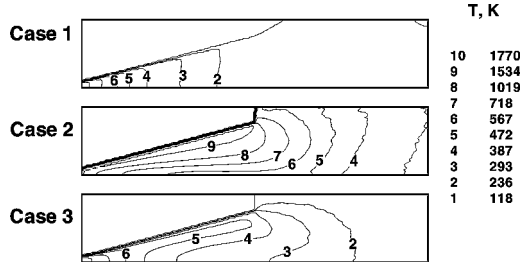

Fig. 7 Translational temperature fields for set 3.

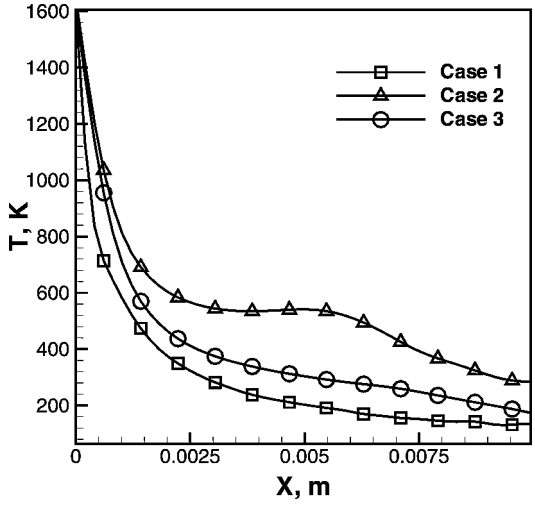

Fig. 8 Translational temperature along the nozzle centerline for set 3.

the efficiency is 17.3% lower than in the ideal case caused by surface friction. Finally, in case 3 thrust performance is lower by 27% as a result of the friction and heat-transfer losses. The specific impulse for the heated flow is higher than that for the cold gas flow, but the efficiency is much lower as a result of additional heat-transfer losses.

High-Temperature Flow

The nozzle flow with a stagnation temperature of 2000 K was calculated using different surface models. The translational temperature contours (Fig. 7) show a significant difference in the flowfields calculated with different surface models. Calculated temperature profiles along the nozzle centerline are plotted in Fig. 8. In the high-temperature case the difference between the adiabatic wall model and a constant wall temperature (case 3) increases.

Calculated performance characteristics for this case are given in Table 4. When the baseline case 3 surface model is used, the specific impulse in the high-temperature gas flow is about two times larger than that for the cold gas.

Figure 9 shows a plot of thrust vs axial station for all three sets of throat conditions for a constant wall-temperature model. The axial distance is normalized by the throat radius, and the thrust is normalized by its value at the throat. In the cold gas case the thrust is increased a maximum of 22%, whereas in the heated and high-temperature cases the maximum value of thrust is only 10 and 7.5% larger than that at the throat. Therefore, for a high stagnation temperature a shorter nozzle or a simple sonic nozzle would be more practical at low Reynolds numbers.

It is concluded from these results that the choice of accommodation coefficients in the gas-surface interaction model is important for an accurate numerical prediction of the nozzle performance at low Reynolds numbers. The specific impulse of the high-temperature thruster is, as expected, higher than that of a cold gas thruster. However, heat-transfer losses are significant and need to be considered. The performance of high-temperature nozzles operating at low Reynolds numbers can be optimized by geometric design.

V. Heated Flow in a Three-Dimensional Nozzle

In this section a cold and heated flow in a three-dimensional nozzle is considered where the viscous effects are even more significant than in the axisymmetric case. The surface-to-volume ratio of a flat high-aspect ratio nozzle is larger than in an axisymmetric nozzle, and the surface effects are therefore more pronounced. The nozzle has a square throat, an expansion angle of 15 deg, and an area ratio of 100. The schematic of the nozzle is shown in Fig. 10. A nitrogen flow with stagnation temperatures $T_0 = 300$ and 1000 K is considered. Similar to the axisymmetric flow, the Reynolds number based on the throat width was 2.05×10^2 in both cases. The diffuse

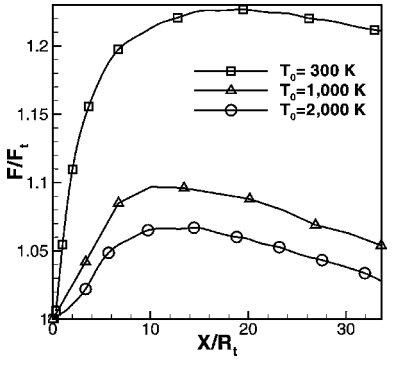

Fig. 9 Normalized thrust at different axial stations for three throat conditions.

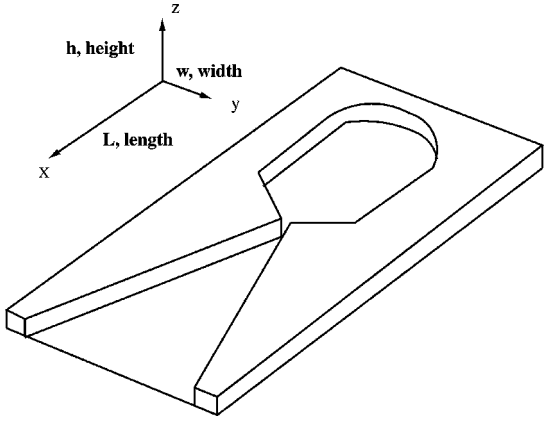

Fig. 10 Schematic of a three-dimensional flat micronozzle.

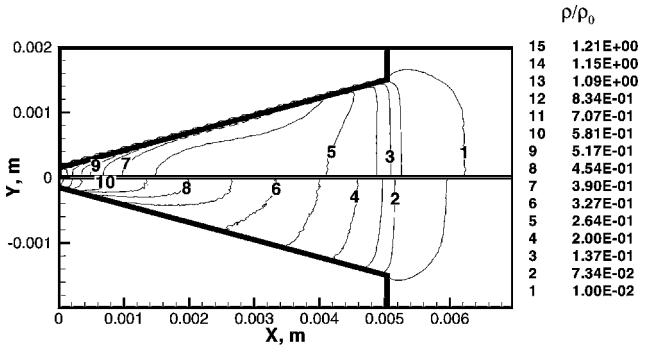

Fig. 11 Normalized density for T_0 = 1000 K (top) and 300 K (bottom).

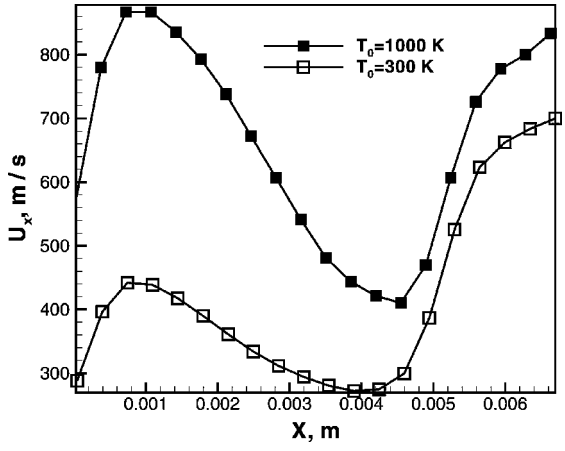

Fig. 12 Velocity in X direction along the nozzle centerline; full accommodation at the wall.

model with a constant wall temperature of 300 K was used for this simulation.

The calculated number density contours in the XY symmetry plane for a cold and heated flow are shown in Fig. 11. The flow structure is different for the two temperature regimes because in the cold gas case the wall temperature is equal to the stagnation temperature, whereas in the heated gas case the wall temperature is lower. In both cases the flow is dominated by the surface. It is illustrated by the profile of velocity in the X direction along the nozzle centerline shown in Fig. 12. The velocity in both cases has a maximum at approximately one-fourth of the nozzle length and after that it drops as a result of viscous dissipation of the flow kinetic energy. The decrease of the velocity at the centerline as a result of wall effects shows that the BL occupies the whole cross-sectional area of the nozzle. The calculated specific impulse is 56.6 and 61.0 s for the cold and heated cases, respectively. The increase of the specific impulse is considerably less than that in the axisymmetric flow as a result of larger surface-area-to-volume ratio.

VI. Hydrogen-Air Propellant Flow in a Conical Nozzle

The performance of an axisymmetric nozzle has been calculated for the exhaust gases of the microcombustor,[3] which uses hydrogen and air. The microcombustor produced temperatures in excess of 1600 K. To simulate the flow in an axisymmetric nozzle for the combustion products generated by a microcombustor, the modeling has been performed for different pressures $p_0 = 0.1$, 0.5, and 1 atm. A stagnation temperature equal to the adiabatic flame temperature will be assumed in the modeling. The product composition was calculated for an equilibrium combustion at a constant pressure and for the stoichiometric fuel-to-oxidizer ratio. Only the major hydrogen-air combustion products, N_2, H_2O, and H_2, were assumed to be present in the nozzle gas flow. The stagnation temperature and species mole fractions are given in Table 5. The flow through an

Table 5 Adiabatic flame temperature and mole fractions for different chamber pressures

p_0, atm	T_{ad}, K	χ_{N2}	χ_{H_2O}	χ_{H_2}
0.1	2302	0.667	0.311	0.022
0.5	2366	0.663	0.320	0.017
1.0	2390	0.661	0.324	0.015

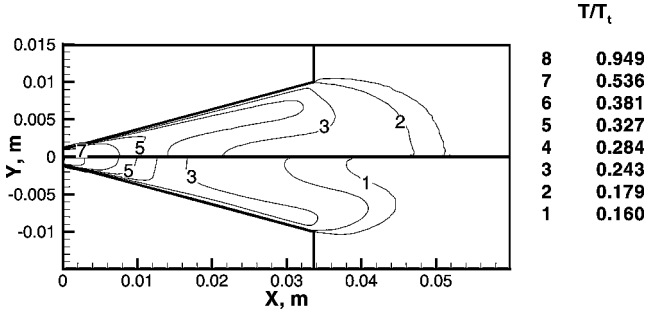

Fig. 13 Translational temperature normalized by its value at the throat for hydrogen-air propellant, conical nozzle, $A = 100$, $\alpha = 15$ deg, $p_0 = 0.1$ atm (top), and $p_0 = 0.5$ atm (bottom).

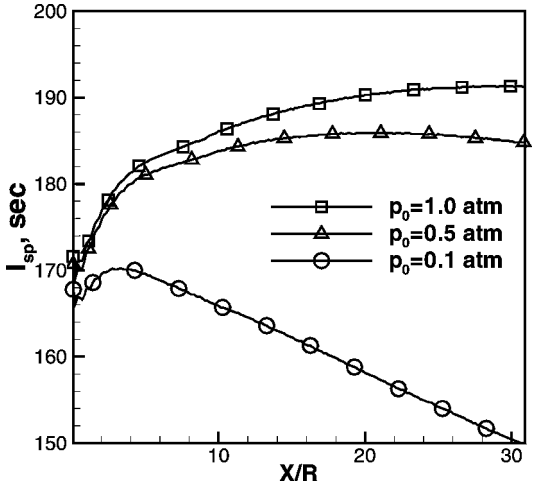

Fig. 14 Specific impulse at different axial stations for different chamber pressures.

axisymmetric nozzle with a throat radius of 1 mm and an area ratio of 100 is simulated, for the Reynolds numbers based on the throat diameter of 208, 1000, and 1976.

Figure 13 shows the calculated translational temperature normalized by its value at the throat for stagnation pressures of 0.1 and 0.5 atm. The temperature fields are similar for the first third of the nozzle. Further downstream, the difference is more pronounced, with the temperature being higher for the less dense case.

The calculated specific impulse at different axial stations is plotted in Fig. 14 for stagnation pressures $p_0 = 0.1$, 0.5, and 1.0 atm. For lower pressures the peak value of I_{sp} is closer to nozzle throat.

Let us now consider the impact of the molecular internal degrees of freedom. For cold gas thruster conditions rotational relaxation is the dominant internal energy transfer process. In a high-temperature polyatomic gas, though, the excitation of molecular vibrations may become important. To study the possible effect of vibrational-translational (VT) energy transfer, the temperature-dependent and constant values of relaxation numbers Z_r ($Z_r = 5$) and Z_v in the Larsen–Borgnakke model have been used in the calculations.

Modeling of temperature-dependent water vibrational relaxation was performed using Eq. (3) of Ref. 17 assuming water molecules have three vibrational modes with one characteristic temperature of 2258 K. The corresponding $Z_v(T)$ changes from 10^4 at 2000 K to 10^6 at 600 K. The vibrational relaxation of H_2O is not well known but is expected to be higher than the slow rates of the temperature-dependent model. Therefore, the constant values of $Z_v = 1$ and 100 were used that correspond to very fast and moderate rates of VT transfer.

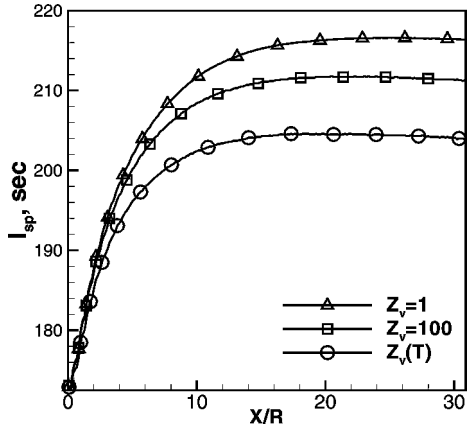

Fig. 15 Specific impulse at different axial stations for $p_0 = 1$ atm and different vibrational relaxation numbers.

Figure 15 shows the calculated specific impulse for $p_0 = 1$ atm and different relaxation numbers. It is seen that there is a significant difference (about 5%) in the results depending on the vibrational energy relaxation number. As expected, a faster VT relaxation increases the transfer of flow internal energy into kinetic energy and thus increases the nozzle performance.

VII. Conclusions

Nozzle flows at low Reynolds numbers, between 2×10^2 and 2×10^3, were modeled for different temperature regimes (stagnation temperature of 300, 1000, and 2000 K). The SMILE computational tool based on the DSMC method was used in the calculations.

The results of the thrust efficiency calculations with different gas-surface interaction models were compared with reported experimental data for a heated nitrogen flow (stagnation temperature of 1033 K). Good agreement was observed when a constant wall temperature of 500 K and a diffuse reflection with complete energy and momentum accommodation coefficients were used in the computations.

The influence of the gas-surface interaction model was examined for an axisymmetric nozzle through variations of energy and momentum accommodation coefficients in three temperature regimes. The selection of the surface model is shown to be more important for a high-temperature nozzle flow at a low Reynolds number of 4.10×10^2. In a high-temperature flow the difference in I_{sp} caused by variations of the energy accommodation coefficient is 18%. In a cold gas flow, where the stagnation temperature is close to the wall temperature, the variation of the energy accommodation coefficient does not significantly change the nozzle efficiency. The choice of momentum accommodation coefficient is important for all temperature regimes. Its impact on thruster efficiency is slightly dependent on the stagnation temperature, at a fixed Reynolds number. The specific impulse was shown to be two times larger for the stagnation temperature of 2000 K than for the 300 K case, and the efficiency is only 10% smaller for the higher temperature case.

A three-dimensional nozzle configuration was studied for two temperature regimes. The most important conclusion related to this case is that the specific impulse increases only a few percent for a heated gas caused by significant heat losses to the wall. In the three-dimensional case the increase in stagnation temperature did not provide a similar increase in the thrust as was found in axisymmetric case.

Hydrogen-air combustion products (a mixture of H_2O, N_2, and H_2) expanding through a conical nozzle were calculated for chamber pressures from 0.1 to 1 atm. The specific impulse of 200 s was obtained for a 1 atm chamber pressure and 150 s for 0.1 atm. The

impact of the translational-vibrational relaxation rate dominated by energy transfer between water and N_2 and H_2 was studied and shown to significantly affect the specific impulse.

This work has demonstrated the utility of DSMC modeling to evaluate small-scale devices such as combustion and nozzle design options. Moreover, it demonstrated that DSMC can be used as an effective design tool to assist in device fabrication and testing.

References

[1]Janson, S. W., Helvajian, H., and Breuer, K., "MEMS, Microengineering and Aerospace Systems," AIAA Paper 99-3802, June 1999.

[2]Bayt, R. L., Breuer, K. S., Lin, L., Forster, F. K., Aluru, N. R., and Zhang, X., "Viscous Effects in Supersonic MEMS-Fabricated Micronozzles," *Proceedings of Micro-Electro-Mechanical Systems (MEMS)—1998. ASME International Mechanical Engineering Congress and Exposition*, American Society of Mechanical Engineers, New York, 1990, pp. 117–123.

[3]Mehra, A., Ayon, A., Waitz, I. A., and Schmidt, M. A., "Microfabrication of High-Temperature Silicon Devices Using Wafer Bonding and Deep Reactive Ion Etching," *Journal of Micromechanical Systems*, Vol. 8, No. 2, 1999, pp. 152–159.

[4]Boyd, I. D., Jafry, Y., and Vanden Beukel, J., "Particle Simulation of Helium Microthruster Flows," *Journal of Spacecraft and Rockets*, Vol. 31, No. 2, 1994, pp. 271–277.

[5]Chung, C.-H., Kim, S. C., Stubbs, R. M., and De Witt, K. J., "Low-Density Nozzle Flow by the Direct Simulation Monte Carlo and Continuum Methods," *Journal of Propulsion and Power*, Vol. 11, No. 1, 1995, pp. 64–70.

[6]Ivanov, M. S., Markelov, G. N., Wadsworth, D. C., and Ketsdever, A. D., "Numerical Study of Cold Gas Micronozzle Flows," AIAA Paper 99-0166, Jan. 1999.

[7]Markelov, G. N., and Ivanov, M. S., "Numerical Study of 2D/3D Micronozzle Flows," *Proceedings of 22nd Symposium on Rarefied Gas Dynamics*, American Inst. of Physics, 2000.

[8]Alexeenko, A. A., Collins, R. J., Gimelshein, S. F., and Levin, D. A., "Numerical Modeling of Axisymmetric and Three-Dimensional Flows in MEMS Nozzles," AIAA Paper 2000-3668, July 2000; *AIAA Journal* (accepted for publication).

[9]Zeleznik, D., Micci, M. M., and Long, L. N., "Direct Simulation Monte Carlo Model of Low Reynolds Number Nozzle Flows," *Journal of Propulsion and Power*, Vol. 10, No. 4, 1994, pp. 546–553.

[10]Murch, C. K., Broadwell, J. E., Silver, A. H., and Marcisz, T. J., "Low-Thrust Nozzle Performance," AIAA Paper 68-17513, Jan. 1968.

[11]Bird, G. A., *Molecular Gas Dynamics and Direct Simulation of Rarefied Gas Flows*, Oxford Univ. Press, New York, 1994.

[12]Ivanov, M. S., Markelov, G. N., and Gimelshein, S. F., "Statistical Simulation of Reactive Rarefied Flows: Numerical Approach and Applications," AIAA Paper 98-2669, June 1998.

[13]Ivanov, M. S., and Rogazinsky, S. V., "Analysis of Numerical Techniques of the Direct Simulation Monte Carlo Method in the Rarefied Gas Dynamics," *Soviet Journal of Numerical Analysis and Mathematical Modeling*, Vol. 2, No. 6, 1988, pp. 453–465.

[14]Koura, K., and Matsumoto, H., "Variable Soft Sphere Molecular Model for Inverse-Power-Law of Lennard-Jones potential," *Physics of Fluids A*, Vol. 3, No. 10, 1991, pp. 2459–2465.

[15]Borgnakke, C., and Larsen, P., "Statistical Collision Model for Monte Carlo Simulation of Polyatomic Gas Mixture," *Journal of Computational Physics,* Vol. 18, No. 4, 1975, pp. 405–420.

[16]Parker, J. G., "Rotational and Vibrational Relaxation in Diatomic Gases," *Physics of Fluids*, Vol. 2, No. 4., 1959, pp. 449–462.

[17]Millikan, R. C., and White, D. C., "Systematics of Vibrational Relaxation," *Journal of Chemical Physics*, Vol. 39, No. 12, 1963, pp. 3209–3213.

[18]Lumpkin, F. E., III, Haas, B. L., and Boyd, I. D., "Resolution of Differences Between Collision Number Definitions in Particle and Continuum Simulations," *Physics of Fluids A*, Vol. 3, No. 9, 1991, pp. 2282–2284.

[19]Haas, B. L., Hash, D. B., Bird, G. A., Lumpkin, F. E., III, and Hassan, H. A., "Rates of Thermal Relaxation in Direct Simulation Monte Carlo Methods," *Physics of Fluids*, Vol. 6, No. 6, 1994, pp. 2191–2201.

[20]Cohen, C. B., and Reshotko, E., "The Compressible Laminar Boundary Layer with Heat Transfer and Arbitrary Pressure Gradient," NACA Rept. 1294, 1956.